Geo-Mar Lett
DOI 10.1007/s00367-010-0192-0

ORIGINAL

# Active mud volcanoes on the upper slope of the western Nile deep-sea fan—first results from the P362/2 cruise of R/V *Poseidon*

**Tomas Feseker · Kevin R. Brown · Cecile Blanchet · Florian Scholz · Marianne Nuzzo · Anja Reitz · Mark Schmidt · Christian Hensen**

Received: 8 July 2009 / Accepted: 26 January 2010


**Abstract** In February 2008, cruise P362/2 was undertaken aboard R/V *Poseidon* to the Giza and North Alex mud volcanoes (MVs) on the upper slope of the western Nile deep-sea fan. Emitted fluids were strongly depleted in chloride and rich in hydrocarbons, predominantly of thermogenic origin. In-situ sediment temperature measurements indicate extremely high and moderate levels of activity for the North Alex MV and Giza MV, respectively, and suggest rapid changes from dormant to active stages. Both the physical properties of core sediments (e.g., color and magnetic susceptibility), and their assemblages of micro- and nannofossils point to different sources for the two mud volcanoes. Biostratigraphic dating suggests source depths of 2,100–2,450 mbsf for the Giza MV and 1,150–1,550 mbsf for the North Alex MV. Very high temperatures of up to 70°C in shallow sediments at the North Alex MV can be explained only if the fluid source were warmer and deeper than the sediment source.

## Introduction

Submarine mud volcanoes have been discovered all over the world on both active and passive margins (Kopf 2002). Sediment fluidization at depths of up to several kilometers below the seafloor is driven by the intense production or influx of fluids and hydrocarbon gases (Hedberg 1974; Brown 1990; Dählmann and de Lange 2003). Despite extensive investigations dealing with mud volcanoes of the Costa Rica continental margin (e.g., Hensen et al. 2004; Schmidt et al. 2005), the Gulf of Cadiz (e.g., Stadnitskaia et al. 2006a; Hensen et al. 2007; Nuzzo et al. 2008), the Sorokin Trough in the Black Sea (e.g., Stadnitskaia et al. 2006b; Feseker et al. 2009a), the Gulf of Mexico (e.g., Reitz et al. 2007), the Arctic (de Beer et al. 2006; Kaul et al. 2006; Feseker et al. 2008; Perez-Garcia et al. 2009), and the Eastern Mediterranean (e.g., The MEDINAUT Shipboard Scientific Party et al. 2001; Aloisi et al. 2002; Bouloubassi et al. 2006; Dupré et al. 2007; Gontharet et al. 2007; Mastalerz et al. 2007; Feseker et al. 2009b) in recent years, the complex geochemical, geological, and microbial processes driven by mud and fluid extrusion at mud volcanoes are not yet fully understood. As mud volcanoes act as conduits for the leakage of fluids, petroleum, and hydrocarbon gases from reservoirs, their study constitutes a promising means for the preliminary characterization of deep-seated resources (e.g., Mastalerz et al. 2007), and the monitoring of geochemical processes and fluid flow occurring in buried sediments (e.g., Hensen et al. 2004). Detailed assessments have shown that unique ecosystems fueled by methane seepage develop at most mud volcanoes (e.g., Werne et al. 2004; de Beer et al. 2006). Even though microbial communities that oxidize methane to $CO_2$ (coupled with the reduction of seawater sulfate) act as a filter to mitigate the emission of this powerful greenhouse gas to the hydrosphere (Niemann et al. 2006), it has been shown that methane emitted from shallow mud volcanoes and cold seeps reaches the mixed layer in the upper water

**Electronic supplementary material** The online version of this article (doi:10.1007/s00367-010-0192-0) contains supplementary material, which is available to authorized users.

T. Feseker (✉) · K. R. Brown · C. Blanchet · F. Scholz · M. Nuzzo · A. Reitz · M. Schmidt · C. Hensen
Marine Biogeochemistry / Marine Geosystems, IFM-GEOMAR, Leibniz Institute of Marine Sciences at Kiel University, Wischhofstr. 1–3,
24148 Kiel, Germany
e-mail: tfeseker@ifm-geomar.de

Published online: 18 February 2010

column at some sites (Schmale et al. 2005; Sauter et al. 2006), in particular at mud volcanoes on the Nile deep-sea fan (Mastalerz et al. 2007). In order to quantify the role of mud volcanoes in global methane budgets, it is important to better understand the processes that control their activity (cf. Wallmann et al. 2006). Despite the fact that some mud volcanoes, such as the Håkon Mosby mud volcano on the Barents Sea slope, have been investigated for years, little is known about temporal variations of mud volcano activity (Feseker et al. 2008).

The Giza mud volcano (Giza MV) and North Alex mud volcano (North Alex MV) are located in the vicinity of designated gas production wells on the upper slope of the western Nile deep-sea fan. Within the framework of the West Nile Delta Project at IFM-GEOMAR, Kiel, these two mud volcanoes were selected for detailed investigation aiming to provide new insights into the dynamics of these unique seafloor features, and their relation to gas reservoirs. Main objectives of the research cruise P362/2 onboard the R/V *Poseidon* in February 2008 included the recovery of sediments for geochemical analyses of pore fluids and light volatile hydrocarbon gases, paleontological characterization of sediment samples, and in-situ sediment temperature measurements along transects across the mud volcanoes. While more than 100 stations were investigated in all during the cruise, this paper focuses on data obtained from gravity cores and in-situ temperature measurements from the central areas of both mud volcanoes. Sedimentological and biostratigraphical analyses, geochemical porewater data, and in-situ temperature and thermal conductivity measurements are comparatively examined to provide first insights into the sediments, fluids, and hydrocarbon gasses, as well as the evolution and eruption history of the Giza and North Alex mud volcanoes.

## Geological setting

The Nile deep-sea fan is the most important sedimentary accumulation in the Eastern Mediterranean. Two geophysical mapping campaigns conducted in 1998 (Prismed II) and 2000 (Fanil) resulted in a first detailed morphostructural description of this deep-sea fan (Mascle et al. 2001; Loncke et al. 2002, 2004), and led to the discovery of several circular and sub-circular sedimentary structures on the upper slope. Up to a few kilometers in diameter and generally showing a low relief of a few tens of meters, these mud volcanoes or so-called mud pies have been interpreted as surface expressions of deep-seated gas chimneys (Loncke et al. 2002, 2004), related to faults and controlled by the tectonic regime (Dupré et al. 2007). Some are known to emit chloride-depleted fluids (Feseker et al. 2009b), and are associated with large methane plumes in the water column (Mastalerz et al. 2007). For a detailed structural analysis of the Nile deep-sea fan, the reader is referred to Loncke et al. (2006). Dupré et al. (2007) provided a comprehensive summary of previous investigations on active gas chimneys on the Nile deep-sea fan, including the North Alex MV. Mineralogical analyses on authigenic carbonates from this mud volcano were presented by Gontharet et al. (2007).

Both the Giza and North Alex MVs are situated on the upper slope of the western province of the Nile deep-sea fan, at 26 and 30 nautical miles (n.m.) from the Egyptian coast, respectively (Fig. 1). The Giza MV is located at 31° 40.51′N and 029°45.00′E at a water depth of about 700 m. It is a circular structure about 2,500 m in diameter (Fig. 2). The highest point is elevated approx. 40 m above the slope, and forms a distinct summit on an otherwise flat plateau at the top of the mud volcano, slightly southeast of the geometrical center. A narrow moat separates the flanks of the mud volcano from the surrounding seafloor. The northwestern part of the moat is interrupted by an approx. 500-m-wide gap that could be the result of slope failure on the flank, possibly due to mud expulsion.

The North Alex MV is located at 31°58.19′N and 030° 08.21′E at a water depth of about 500 m, approx. 26 n.m. to the northeast of the Giza MV. Situated within a caldera-like structure that is about 3,000 m in diameter, this mud volcano has a diameter of less than 2,000 m and (at its highest point) an elevation of nearly 50 m above the surrounding seafloor (Fig. 3). The central plateau is characterized by gentle slopes extending to a steep edge of about 40 m. Based on a geophysical mapping campaign, the North Alex MV was described as a deep-rooted active gas chimney that may have triggered slope destabilization associated with significant northward sediment flows and slumps, following the local slope gradient (Loncke et al. 2004). Further investigations in 2003 showed a moderate sediment temperature anomaly of about 0.8°C $m^{-1}$ and sporadic gas ebullition at the center (Dupré et al. 2007), indicative of a minor level of activity.

## Materials and methods

The positioning of all winch-operated tools at the seafloor was controlled using a GAPS-transponder attached to the cable approx. 50 m above the instrument. For the North Alex MV, the resulting positioning error is estimated at about 5–10 m. Due to a failure of the GAPS system during the work at the Giza MV, however, the accuracy of positioning was reduced to about 20–30 m.

### Sediment sampling and core logging

Surface and subsurface sediment samples were retrieved using a gravity corer equipped with a 5.75-m-long barrel.

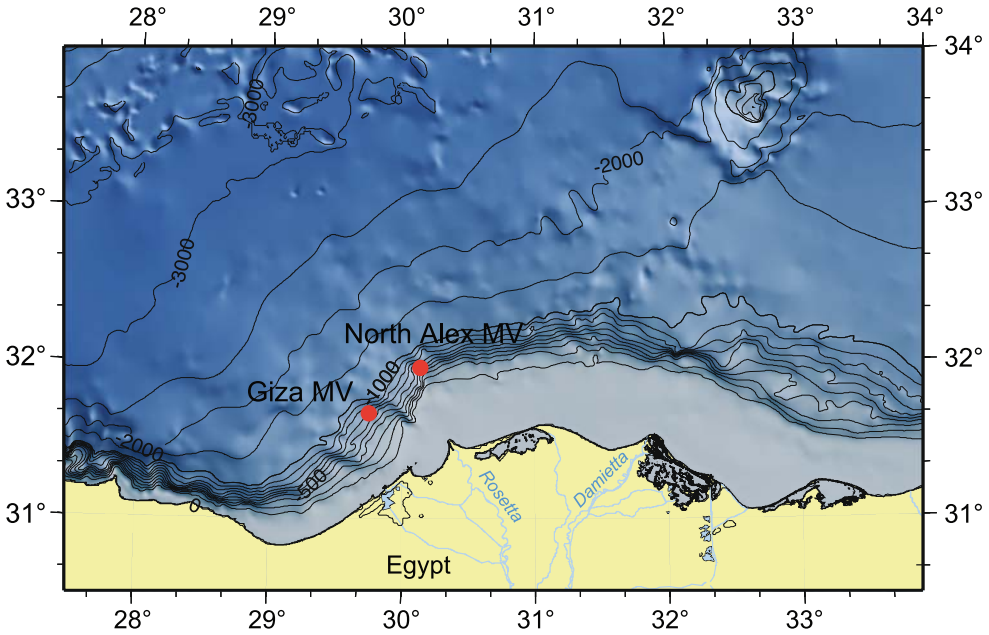


**Fig. 1** Locations of the Giza MV and North Alex MV on the upper slope of the western Nile deep-sea fan, approx. 30 n.m. from the Egyptian coast

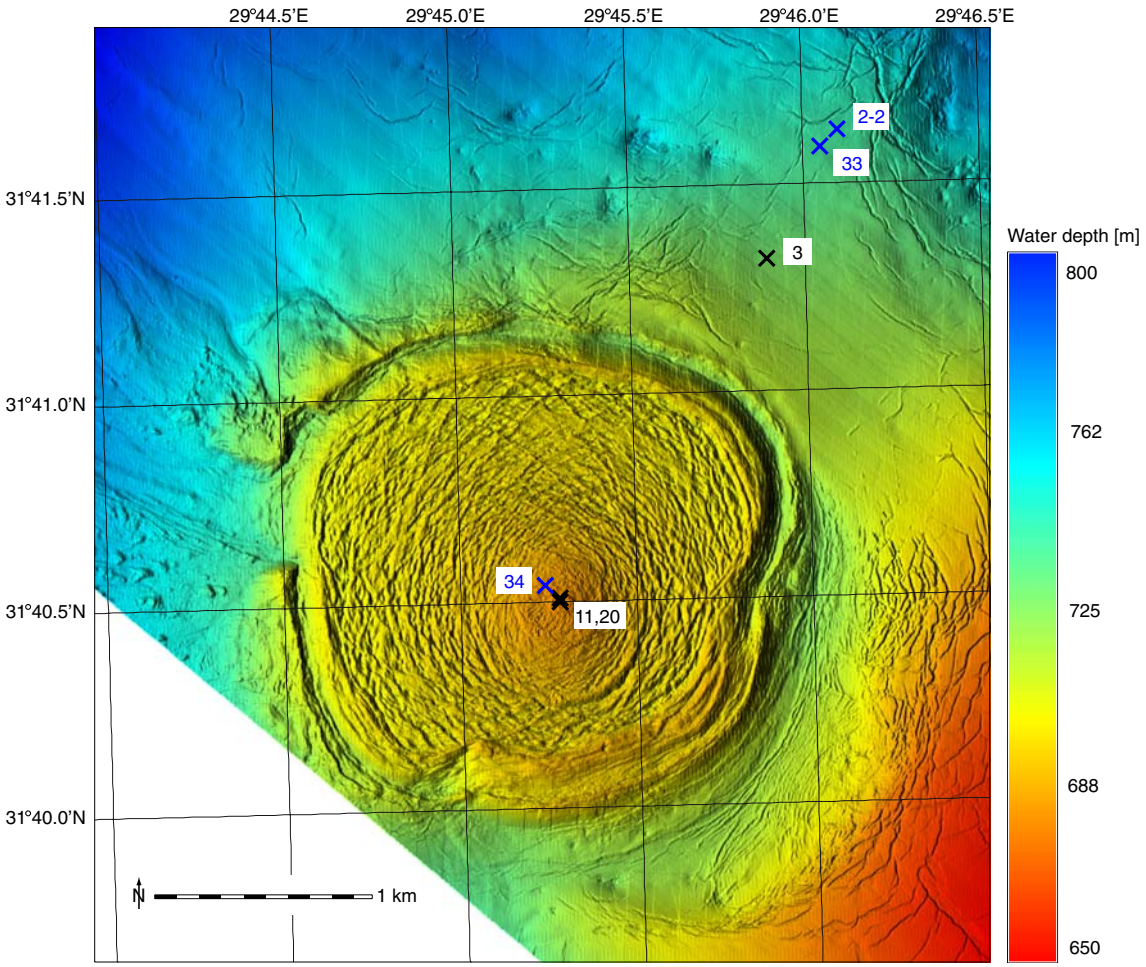


**Fig. 2** Shaded bathymetric map of the Giza MV showing the locations of gravity cores (*blue crosses*) and in-situ sediment temperature measurements (*black crosses*) taken in the central area of the mud volcano during the P362/2 cruise of R/V *Poseidon* in February 2008 (DTM courtesy of BP Ltd.)

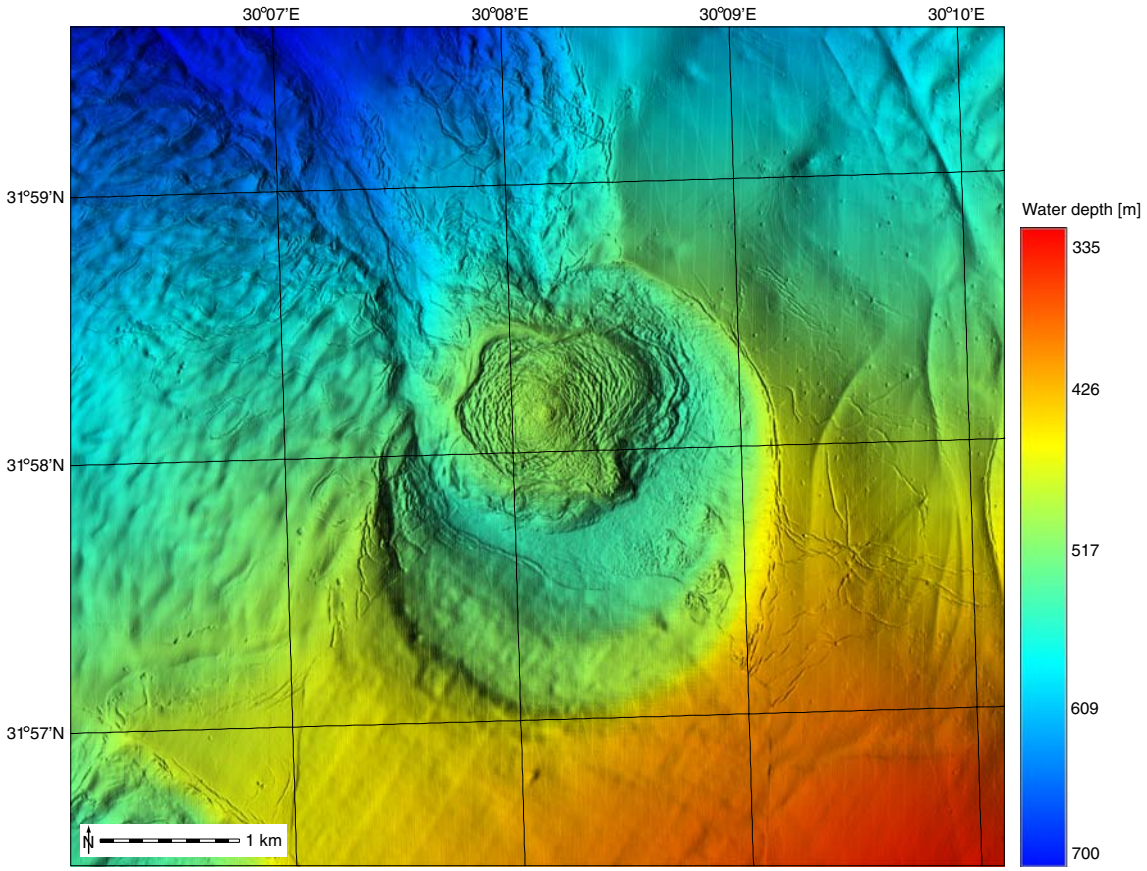


**Fig. 3** Shaded bathymetric map of the North Alex MV and surrounding seafloor (DTM courtesy of BP Ltd.)

The data presented here are based on one core from the center of the Giza MV (P362/2–34), one core from the center of the North Alex MV (P362/2–100), and two cores from a reference site approx. 1.3 n.m. NE of the Giza MV (P362/2–2–2 and P362/2–33). The locations of the gravity corer stations are shown in Figs. 2 and 4.

The cores were subdivided into 1-m sections and cut lengthwise. Sediment visual description was then carried out in order to detect any changes in sediment color (using a Munsell color chart), sediment texture, and sedimentary structures. The split sections were stored at 4°C until they were logged using a GEOTEK Ltd. multi-sensor core logger (MSCL) to assess the physical properties of sediments after the cruise. Magnetic susceptibility, P-wave velocity, and bulk density were measured every 1 cm by pushing the section through a series of online sensors using a stepper motor controlled by a computer terminal. The volume-specific magnetic susceptibility was obtained by means of a Bartington Instruments Ltd. magnetic susceptibility meter coupled to a MS2-E point sensor. This provides a reliable estimation of the magnetic mineral content, and is particularly influenced by the amount of ferromagnetic (oxi)hydroxides like magnetite ($Fe_3O_4$). The P-wave velocity is obtained by measuring the travel time of a P-wave pulse between the vertically aligned transducer and receiver. This measurement is here used to estimate the sediment thickness in the core liner, with respect to a known reference core thickness.

The gamma-ray attenuation bulk density was obtained by measuring the attenuation of incident gamma-rays through the core, between a $^{137}Cs$ source (beam of 5 mm, energy of 0.662 MeV) and a detector. The wet bulk density $\rho$ is estimated using the relationship $\rho = (1/m^{*}d)^{*} \ln(I_0/I)$, where $m$ is the attenuation rate, $d$ the sediment thickness, $I_0$ the initial gamma-ray intensity, and $I$ the measured intensity. Due to similar attenuation coefficients for most common minerals and aluminum, bulk density is obtained through direct calibration of the densitometer using aluminum rods of different diameters mounted in a core liner that is filled with distilled water. Wet bulk density is influenced mainly by sediment texture, mineralogy, and compaction (grain fabric).

## Micropaleontological sampling and analyses

Sediment samples of 10 ml volume were taken at various intervals from the cores collected at the Giza and North Alex MVs. The samples were weighed, then freeze dried

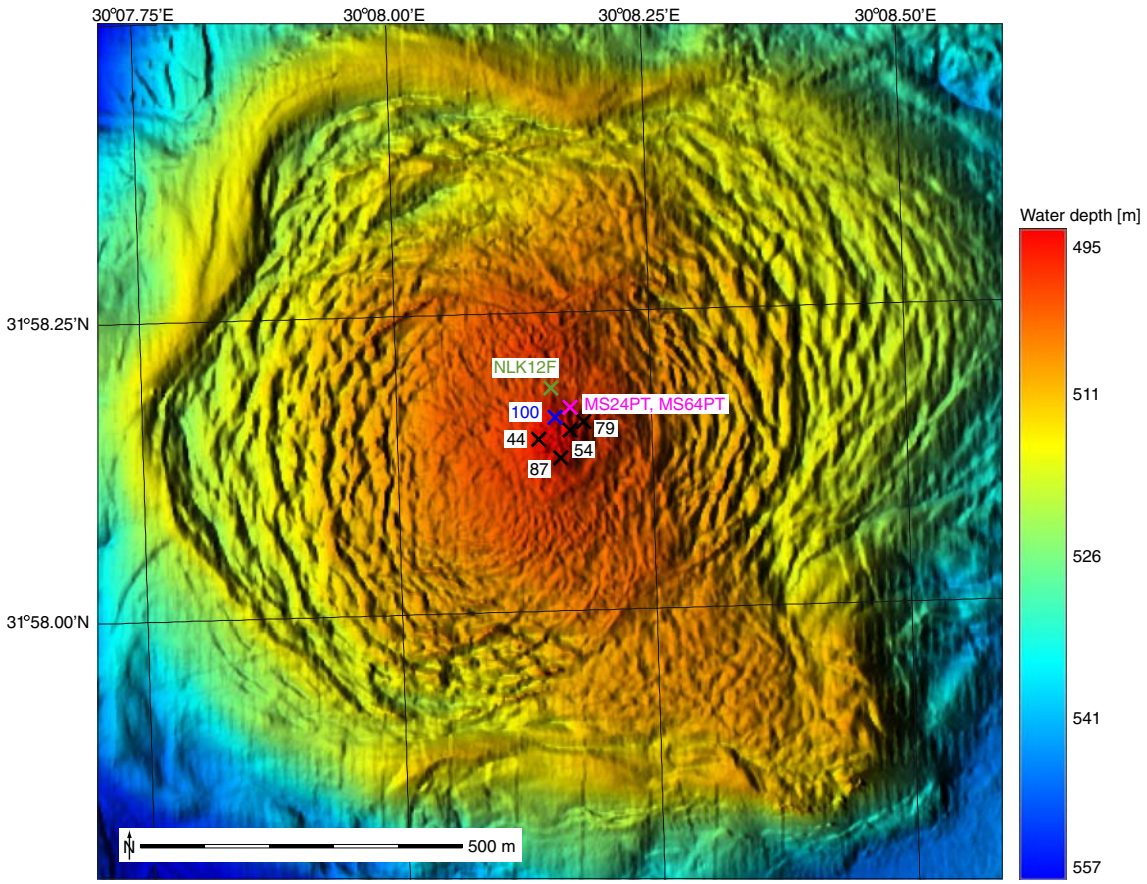


**Fig. 4** Shaded bathymetric map of the central North Alex MV showing the locations of the gravity core (*blue cross*) and in-situ temperature measurements (*black crosses*) taken in the central area during the P363/2 cruise of R/V *Poseidon* in February 2008. The green and pink crosses indicate the locations of in-situ sediment temperature measurements during the Nautinil cruise of R/V *L'Atalante* in September 2003, and the Mimes cruise of R/V *Pelagia* in June/July 2004, respectively (DTM courtesy of BP Ltd.)

prior to washing with fresh water through a 62-μm sieve. The washed residues were oven dried at 50°C, followed by weighing and then dry sieving at 125 μm; a sample splitter served to obtain aliquots. From complete aliquots of each sample, at least 300 planktonic foraminifer specimens were hand-picked under a binocular microscope using a moistened brush. Determination of foraminiferal species and ranges was made with reference to Stainforth et al. (1975), Iaccarino (1989), and Bolli and Saunders (1989).

After all other sampling had been completed, clasts were obtained by washing the remaining core material through a 1-mm sieve. The clasts were rinsed in fresh water before being oven dried. Several clasts with sizes greater than 2 cm were selected from each section of the cores. The surface was first scraped with a scalpel to remove loose attached material. A small amount of material was then scraped from the clasts with the scalpel onto a glass cover slip. The scrapings were mixed with demineralized water to produce a thin suspension, which was spread across the entire surface of the cover slip and allowed to dry. The cover slip was then fixed onto a glass slide using Norland Optical Adhesive. Identification of coccoliths was carried out by means of a Zeiss Axioplan at various magnifications. Identification of nannofossils was made with reference to Perch-Nielsen (1989); nannofossil biozonation is based on Martini (1971).

## Geochemical porewater and gas sampling and analyses

Immediately after opening the gravity cores, 2–5 cm thick sediment samples were taken in 15–40 cm intervals. Porewater recovery was done in a cooled laboratory at in-situ temperature (12°C), using an argon gas pressure squeezer at 2–5 bars combined with filtering through cellulose acetate filters (0.2 μm). Porewater light volatile hydrocarbon gases were stripped from sediments according to the method of McAullife (1971). Sediment plugs were recovered using a clean 10-ml, disposable polypropylene syringe that had the end cut off. The sediment plug was immediately injected into a 30-ml glass vial filled with 10 ml of a 10% aqueous solution of potassium chloride (KCl). The vial was sealed and then vigorously shaken to

disaggregate the fine-grained material ("mud"), and to stop all bacterial activity due to KCl poisoning (Bowes and Hornibrook 2006). The sample was allowed to equilibrate with the vial headspace for 24–48 h. The gas was extracted in a syringe by injecting an equivalent amount of 10% KCl solution. The headspace gas was later transferred into a sterile 20-ml serum vial filled (bubble-free) with a pH 1, 10% KCl solution, by displacement of an equivalent amount of solution. The vials were stored upside down in order to minimize potential exchange with air through the septum.

The total alkalinity (TA) of the porewater was determined by titration with HCl using the Tashiro indicator, a mixture of methyl red and methylene blue (Ivanenkov and Lyakhin 1978). The titration vessel was bubbled with nitrogen to strip any $CO_2$ and $H_2S$ produced during the titration. Chloride concentrations were determined applying a Mohr titration with $AgNO_3$ (Gieskes et al. 1991). The latter two methods were calibrated with IAPSO seawater standard. Porewater sub-samples were analyzed for sodium and sulfate by ICP-AES and ion chromatography, respectively, in shore-based laboratories at IFM-GEOMAR. Methane concentrations were determined by gas chromatography-flame ionization chromatography (GC-FID) at IFM-GEOMAR.

### In-situ temperature and thermal conductivity measurements

#### *Heatflow probe*

In-situ sediment temperature and thermal conductivity were measured using a standard heatflow probe in the violin bow design after Bullard (1954), manufactured by FIELAX GmbH in Bremerhaven, Germany. The heatflow probe is equipped with 22 thermistors distributed regularly over an active length of 5.67 m. The resolution of the thermistors is better than 0.001°C; they were calibrated to a platinum resistance thermometer, obtaining an accuracy of about 0.002°C over a temperature range of −2 to 60°C. At each station, the probe was left in the sediment for at least 7 min after penetration to allow the sensors to adjust to ambient temperature. During this time, temperature readings from all sensors were recorded at an interval of 1 s, and the equilibrium sediment temperatures at the depths of the sensors were calculated by extrapolation from the time series. Sensors for tilt, acceleration, and pressure helped to evaluate the data more precisely.

At selected stations, initial recording of sediment temperature profiles during the first 7 min were followed by conductivity measurements. A controlled heat pulse was exerted into the sediment through a heater wire along the entire active length of the probe, and the thermal conductivity of the sediment was determined via the decay of the heat pulse during the next 7 min.

#### *Temperature loggers mounted on gravity corer*

In addition to temperature measurements using the heatflow probe, autonomous miniaturized temperature loggers (MTLs) were applied to assess the temperature regime from which the gravity cores were taken. During most deployments of the gravity corer, three MTLs mounted on outriggers were attached to the corer barrel. Each MTL measures at a resolution better than 0.001°C; the MTLs were calibrated to an accuracy of about 0.002°C prior to the cruise, over a temperature range of −5 to 55°C. At each station, the gravity corer remained in the sediment for at least 7 min, during which the adjustment of the sensors to ambient temperature was recorded at an interval of 5 s. Equilibrium temperatures were calculated by extrapolation from the time series in the same way as for the heatflow probe. The MTLs were mounted at distances of 0.47, 2.70, and 4.64 m from the tip of the corer barrel. An additional tilt sensor mounted close to the top of the gravity corer was used to verify the penetration angle.

## Results

### Sedimentology

Cores P362/2–34 and P362/2–100, which were collected from the centers of both mud volcanoes, contain brownish to greenish gray-colored silty-clayey mud breccias, and large amounts of consolidated clasts (Table 1). Sediments from the North Alex MV are darker and greener than those from the Giza MV. Three main classes of clasts are evident: (1) mudstones, which contain fine material of a nature similar to that of unconsolidated mud, (2) sandstones, which contain coarser material of varying mineralogy, and (3) carbonate precipitates, present only in cores from the North Alex MV, and that might correspond to former chimneys. Clast size ranges from millimeter- to centimeter-scale.

Reference cores P362/2–33 and P362/2–2–2 contain silty-clayey sediments of varying colors, from light brown to dark olive gray, and devoid of clasts (Table 1). Sediment color varies at centimeter-scale in the uppermost 50 cm (which is typical of an oxidation front in hemipelagic sediments), and at millimeter-scale below 100 cm, forming laminations. These fine laminations, constituted of alternating horizontal light- and dark-colored layers, occur throughout most of the core, indicating an undisturbed stratigraphy.

Differences between sediments from the Giza MV and North Alex MV are also evident in the physical properties. Sediments from the Giza MV have higher mean magnetic susceptibility and higher bulk density than those from the North Alex MV (Table 1). The detailed physical logs of the

**Table 1** Sedimentological properties of samples from Giza MV, North Alex MV, and the reference site

| | P362/2–34, Giza MV | P362/2–100, North Alex MV | P362/2–33 & P362/2–2–2, reference |
|---|---|---|---|
| Mean density (g $cm^{-3}$) | 1.54 | 1.27 | 1.2 |
| Mean magnetic susceptibility ($10^{-6}$ SI) | 10 | 8.8 | 23.8 |
| Mean color | Dark gray (2.5Y4/1 to 10YR4/1) | Very dark gray (2.5Y3/1) | Gray brown (7.5YR7/3); dark laminae (2.5Y4/1); light laminae (2.5YR8/2) |
| Clasts | Mudstone, sandstone | Mudstone, sandstone, authigenic carbonates | None |

cores are shown in the electronic supplementary material for this article, available online to authorized users. Down-core magnetic susceptibility and bulk density profiles have large-amplitude and high-frequency variations, and are not correlated. Sediments from the reference core have high mean magnetic susceptibility values and low mean density values. Down-core magnetic susceptibility and density profiles are broadly correlated, with higher values at the top of the core.

## Micropaleontology

The details of sediment samples used for biostratigraphical analyses, and the counts of all identified foraminifer species are provided in the online electronic supplementary material for this article. The stratigraphic ranges of all the species identified within the samples are shown in Fig. 5. The main micropaleontological differences and similarities between the samples from the two mud volcanoes can be seen clearly when the identified species are grouped by their first occurrence in the fossil record (Fig. 6): the samples from both mud volcanoes are dominated by long-ranging species, including *Globigerinoides ruber*, *Globigerinoides trilobus*, *Globigerina bulloides*, and *Globigerinita glutinata*. Samples from both mud volcanoes contain similar percentages of Pleistocene species, but they differ in the percentage of Pliocene and Miocene species.

### *Giza MV*

The presence of *Globorotalia truncatulinoides excelsa* and *Globigerinella calida* are good indicators of Pleistocene sedimentation (N22/N23). A significant proportion of the samples contain Middle to Late Pliocene foraminiferal species (*Globorotalia crassaformis*, *Globorotalia inflata*, *Globorotalia puncticulata*, *Neogloboquadrina acostaensis*, and *Neogloboquadrina humerosa*). The *G. inflata* specimens have four chambers in the last whorl, which Stainforth et al. (1975) interpret as the Late Pliocene form of the species. The presence of *G. puncticulata* and *G. crassaformis*, but the absence of *Globorotalia margaritae* suggest N20 rather than N19 as the depositional age. Use of the *Neogloboquadrina* genus to define the base of the Pleistocene is not possible, as many show intermediate morphology between *N. acostaensis*, *N. humerosa*, and the younger *N. dutertrei* (Pleistocene) species. The specimens show a low trochospiral coiling, with umbilical-extramarginal aperture, often boarded by a lip, with four to five chambers in the last whorl. The umbilical aperture of *N. dutertrei* is seen only in a few medium-spired specimens. These commonly have five-six chambers in the last whorl, with the last chamber becoming lobate; no specimens have the umbilical tooth diagnostic of *N. dutertrei*. This morphological intergradation makes it difficult to differentiate between *N. acostaensis*, *N. humerosa*, and *N. dutertrei*.

The samples from the Giza MV also contain significant numbers of reworked foraminifers, identified by being deformed or heavily encrusted with hardened matrix material. Thus, positive identification beyond genus was difficult. The flattened specimens were not included in counts of foraminiferal abundance. Identified specimens include large "*Globigerina*", but this identification is based on wall structure and coiling mode only. *Catapsydrax* cf. *martini*, *Globigerinoides bisphericus*, *Dentoglobigerina altispira*, *Globorotalia peripheroronda*, and *Globoquadrina dehiscens* all indicate pre-Messinian deposition in the Middle Miocene (possibly Langhian).

The vast majority of the clasts examined are mudstones, and do not contain nannofossils. Several clasts contain *Calcidiscus macintyrei*, *Discoaster brouweri*, *D. variablilis*, and *Reticulofenestra pseudoumbilica*, which indicate a Late Pliocene to Early Pleistocene time period (NN15–NN18). Three clasts show assemblages that comprise *Cyclicargolith floidanus*, *Helicosphaera kamptneri*, *R. pseudoumbilica*, *D. variabilis*, *D. kugleri*, *Coccolithus miopelagicus*, *Spenolithus moriformis*, and *S. heteromorphus*, indicative of a Middle Miocene depositional age (NN5–NN6).

### *North Alex MV*

The presence of *N. acostaensis* and *N. humerosa*, along with *G. inflata* indicates a Late Pliocene/Early Pleistocene

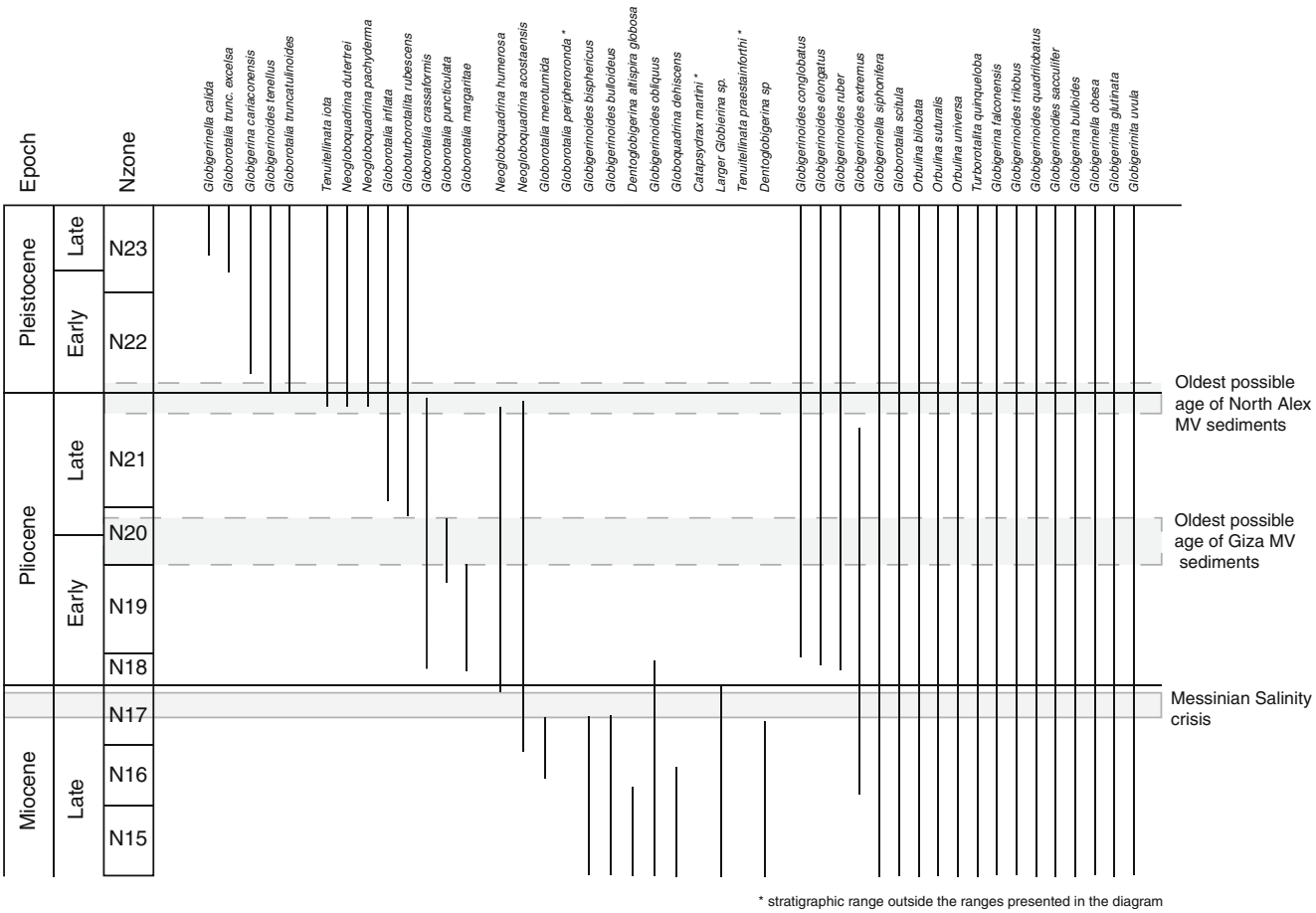


**Fig. 5** Biostratigraphic range chart for all species identified in samples from the Giza MV and North Alex MV. The oldest possible biostratigraphic ages of sediments from the two mud volcanoes are marked by *hatched rectangles*. Foraminiferal N zones follow the scheme of Blow (1969), modified by Bolli and Saunders (1989)

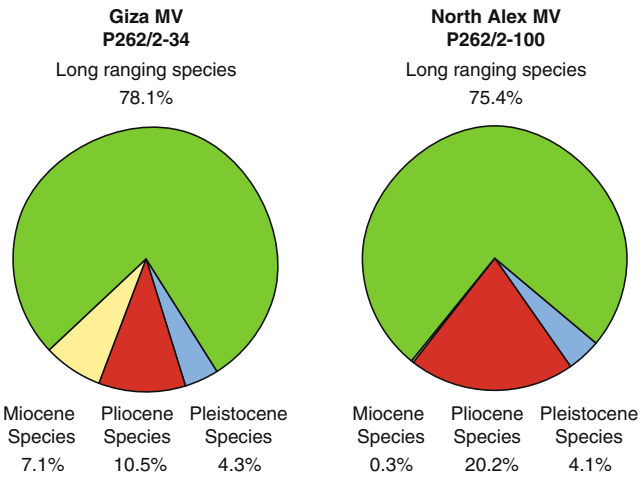


**Fig. 6** Relative abundance of foraminifers for all samples taken from the Giza and North Alex mud volcanoes, grouped by geological epoch of first occurrence

depositional age (N21). The *G. inflata* identified in the North Alex MV samples differ from those in the Giza MV samples, in that they exhibit the typical three-chambered morphology commonly recorded for the Pleistocene. Again, intergradation between *N. acostaensis* and *N. dutertrei* makes positive identification difficult. The presence of *G. truncatulinoides* and *G. calida* is a clear indication of a Pleistocene (N22/N23) age of deposition. In contrast to the samples from the Giza MV, reworked Miocene species were not found in samples from the North Alex MV.

Of the total of 18 clasts that were examined, only five were found to contain nannofossils—*Pseudoemiliania lacunose*, *Helicosphaera sellii*, *C. macintyrei*, *D. brouweri*, and *D. variabilis*, which indicate a Late Pliocene to Early Pleistocene age (NN18–NN19).

### *Reference site*

Reference core P362/2–2–2 consists of Holocene hemipelagic deposits. $^{14}$C dating of *G. ruber* from the core reveals an age of 9,160±90 cal. years at a core depth of

500 cm, and of 7,200±60 cal. years at 100 cm (Lorenzen 2009). Typical Pleistocene species are found throughout the core; *G. ruber* being the dominant species of planktonic foraminifer found within core samples. The core exhibits laminated sediments below a depth of 100 cm, within which no benthic foraminifers were found.

## Geochemistry

Depth profiles of porewater concentrations of sodium/chloride (Na/Cl), chloride (Cl), sulfate ($SO_4$), and methane ($CH_4$), as well as alkalinity in sediments from cores P362/2–100 (North Alex MV), P362/2–34 (Giza MV), and P362/2–2–2 (reference site NW of Giza; Table 2 and Fig. 7) show that the pore fluids become strongly depleted in major seawater ions at greater core depths (cf. chlorinity profiles). This trend is coupled with increasing porewater Na/Cl ratios and alkalinity levels compared to the reference core values (cf. first and last column of Fig. 7). Freshened pore fluids occur immediately below the depth of $SO_4$ penetration, which is generally shallower at the North Alex MV than at the Giza MV (~100 and 150–200 cmbsf, respectively; Fig. 7). In contrast to the reference site, where a linear decrease (and deeper penetration) of $SO_4$ concentration with depth is observed, no concentration gradient is developed in the mud volcano sediments between the bottom seawater and interstitial fluids within the upper 30–150 cmbsf. Below this depth interval, the transition between seawater $SO_4$ concentrations and $SO_4$-depleted fluids in the lower part of the cores is marked by a very steep concentration gradient, which contrasts with the smooth decrease observed at the reference site (Fig. 7). The MV pore fluids are saturated in methane ($CH_4$), with concentrations reaching values of 5 mM. However, in-situ concentrations are probably much higher than the measured values, because of the losses induced by intense outgassing caused by depressurization during core recovery. The pore fluids are also highly enriched in heavier $CH_4$ homologues (ethane to pentanes), and $CH_4/(C_2H_6+C_3H_8)$ ratios have values of ~10 at the North Alex MV (P362/2–100) and ~25 at the Giza MV (P362/2–34; Table 3). At the center of the North Alex MV (P362/2–100), high amounts of $CH_4$ were recorded at all depths, including the first few centimeters below the seafloor. In contrast, $CH_4$ concentrations decrease in the upper part of the cores at all other sites, and the fluids become depleted in $CH_4$ within the first 100 cmbsf (Fig. 7).

## Sediment temperature and thermal conductivity

### *Heatflow probe stations*

In-situ sediment temperature measurements using the heatflow probe were conducted at two stations in the central area of the Giza MV, and at a reference station a few kilometers northeast of this mud volcano (Table 4, Fig. 8; cf. Fig. 2 for station locations). At the reference heatflow station (P362/2–3) the temperature profile is linear, and indicates a temperature gradient of approx. 0.032°C $m^{-1}$. At the center of the Giza MV (P362/2–11 and P362/2–20), the sediment temperatures range from 13.848°C at the seabed to 36.529°C at 5.7 mbsf. Both profiles are in good agreement (Fig. 8), and show a linear temperature increase with depth of about 4°C $m^{-1}$.

Even higher in-situ sediment temperatures were recorded at the four stations in the central area of the North Alex MV (Table 4; cf. bathymetric map in Fig. 4 for station locations). Here, the temperature rises from about 13.888° C at the seabed to more than 50°C at 5 mbsf (Fig. 8). The highest temperature of 68.013°C was recorded at station P362/2–44 at 5.7 mbsf. The difference between individual profiles reaches more than 10°C at a given depth, and the gradients range between 7.13 and 25.89°C $m^{-1}$ for the upper part of the profiles, revealing a very inhomogeneous sediment temperature distribution.

The in-situ thermal conductivity measurements (Table 5) have values ranging from 0.86 to 1.03 W $K^{-1}$ $m^{-1}$, and suggesting a trend from relatively low thermal conductivity in the surrounding seabed to higher conductivity within the mud volcano sediments. Unfortunately, the high temperatures at the center of the North Alex MV made it impossible to measure the thermal conductivity in-situ, because the sediment temperatures rose beyond the detection range of the heatflow probe as soon as a heat pulse was triggered. Combining the results of the conductivity and temperature measurements yields a background regional heatflow of approx. 30 mW $m^{-2}$; the heatflow at the Giza MV and North Alex MV reaches more than 3.5 and 16 W $m^{-2}$, respectively.

### *In-situ temperature measurements at gravity corer stations*

In-situ sediment temperature measurements were conducted during deployments of the gravity corer in the central areas of both mud volcanoes, as well as at the reference site northeast of the Giza MV (Table 6; cf. Figs. 2 and 4 for station locations). It was not attempted to estimate the penetration depth of the gravity corer, i.e., the absolute depths of the temperature measurements. At the reference station (P362/2–33), the sediment temperature difference between the topmost and lowermost sensor corresponds to a temperature gradient of about 0.039°C $m^{-1}$. At station P362/2–34, slightly northwest of the highest point of the Giza MV, the sediment temperatures at the sensors range from 14.18 to 20.783°C, corresponding to a temperature gradient of about 1.58°C $m^{-1}$. At the center of the North Alex MV, the sediment temperature at the lowermost sensor

**Table 2** Results of geochemical porewater analyses

| Depth (cmbsf) | Cl (mM) | Na/Cl | $SO_4$ (mM) | Alkalinity (meq $L^{-1}$) | Depth-$CH_4$ (cmbsf) | $CH_4$ (mM) |
|---|---|---|---|---|---|---|
| Reference core P362/2–2–2 | | | | | | |
| 5.5 | 608 | 0.974 | 32.8 | 2.96 | – | – |
| 19.5 | 614 | 0.862 | 31.7 | 3.88 | – | – |
| 31.5 | 614 | 0.866 | 30.8 | 4.19 | – | – |
| 59.5 | 615 | 0.969 | 29.4 | 5.86 | – | – |
| 84.5 | 612 | 0.972 | 27.9 | 7.47 | – | – |
| 109.5 | 615 | 0.951 | 27.4 | 8.07 | – | – |
| 134.5 | 614 | 0.842 | 26.0 | 9.34 | – | – |
| 159.5 | 616 | 0.858 | 25.4 | 10.15 | – | – |
| 184.5 | 612 | 0.968 | 23.5 | 11.30 | – | – |
| 209.5 | 611 | 0.866 | 23.1 | 11.84 | – | – |
| 234.5 | 614 | 0.834 | 22.0 | 12.76 | – | – |
| 267.5 | 616 | 0.952 | 20.6 | 14.03 | – | – |
| 297.5 | 610 | 0.980 | 19.4 | 15.13 | – | – |
| 325.5 | 614 | 0.950 | 18.3 | 15.80 | – | – |
| 355.5 | 604 | 0.967 | 17.5 | 17.20 | – | – |
| 385.5 | 611 | 0.844 | 16.0 | 17.87 | – | – |
| 415.5 | 609 | 0.844 | 14.8 | 18.93 | – | – |
| 445.5 | 610 | 0.855 | 13.7 | 19.70 | – | – |
| 480.5 | 607 | 0.862 | 12.1 | 20.56 | – | – |
| 515.5 | 616 | 0.960 | 11.5 | 20.56 | – | – |
| Core P362/2–34, Giza MV | | | | | | |
| 2.5 | 614.09 | 0.879 | 32.52 | 2.65 | 10 | 0.1 |
| 21.5 | 615.07 | 0.874 | 32.05 | 2.96 | 30 | 0.0 |
| 41.5 | 607.28 | 0.873 | 32.49 | 2.92 | 50 | 0.1 |
| 62.5 | 611.17 | 0.876 | 32.46 | 2.88 | 70 | 0.0 |
| 81.5 | 618.96 | 0.878 | 32.17 | 2.81 | 90 | 0.1 |
| 101.5 | 618.96 | 0.866 | 32.28 | 2.90 | 110 | 0.1 |
| 121.5 | 603.39 | 0.887 | 31.04 | 3.55 | 130 | 0.0 |
| 141.5 | 550.83 | 0.954 | 16.09 | 14.72 | 150 | 2.9 |
| 170.5 | 492.44 | 0.981 | 0.99 | 27.29 | 160 | 0.8 |
| 176.5 | 490.50 | 0.916 | 0.71 | 30.55 | 178 | 2.2 |
| 199.5 | 229.68 | 1.531 | 0.46 | 38.81 | 208 | 1.1 |
| 219.5 | 165.44 | 1.300 | 0.75 | 38.62 | 228 | 1.9 |
| 239.5 | 154.74 | 1.373 | – | 52.26 | 268 | 2.7 |
| 259.5 | 152.79 | 1.292 | 0.23 | 53.99 | 315 | 2.6 |
| 280.5 | 147.93 | 1.309 | 0.60 | 58.61 | | |
| 299.5 | 146.95 | 1.209 | – | 58.99 | | |
| 319.5 | 144.03 | 1.317 | 0.42 | 60.53 | | |
| Core P362/2–100, North Alex MV | | | | | | |
| 3.0 | 606.31 | 0.889 | 24.989 | 11.59 | 10 | 2.0 |
| 28.0 | 600.47 | 0.886 | 27.561 | 10.06 | 20 | 2.7 |
| 53.0 | 427.24 | 1.010 | 6.678 | 27.98 | 47 | 0.8 |
| 78.0 | 239.41 | 1.115 | 0.701 | 48.48 | 70 | 1.3 |
| 103.0 | 197.56 | 1.145 | 0.219 | 52.12 | 91 | 2.1 |
| 128.0 | 198.53 | 1.087 | 0.08 | 49.63 | 120 | 0.6 |
| 153.0 | 183.94 | 1.164 | 0.115 | 50.59 | 147 | 1.9 |
| 178.0 | 184.91 | 1.176 | 0.183 | 49.25 | 170 | 0.9 |
| 203.0 | 179.07 | 1.220 | 0.031 | 50.20 | 190 | 1.5 |
| 228.0 | 183.94 | 1.197 | 0.0 | 50.01 | 210 | 0.9 |
| 253.0 | 178.10 | 1.218 | 0.033 | 49.44 | 240 | 1.7 |

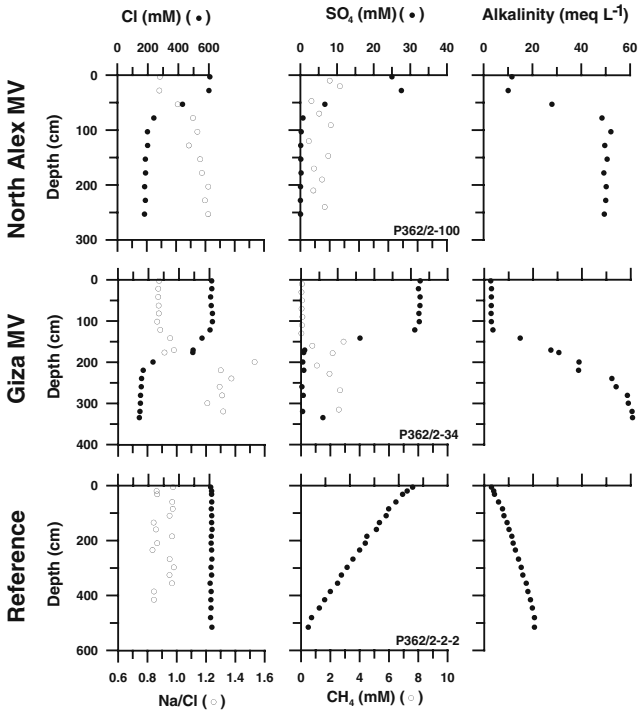


**Fig. 7** Porewater profiles of sodium/chloride (Na/Cl), chloride (Cl), sulfate ($SO_4$), methane ($CH_4$), and alkalinity in sediments from cores P362/2–100 (North Alex MV), P362/2–34 (Giza MV), and P362/2–2–2 (reference site NW of Giza)

exceeded the detection range of the MTL: within a few seconds after penetration, the temperature at the sensor was higher than 55°C. Even the topmost sensor indicated a temperature of 33.94°C in the near-surface sediments.

## Discussion

### Characterization of mud volcano fluids and sediments

The pore fluids and sediments found at the Giza and North Alex mud volcanoes are markedly distinct from those of the surrounding seabed. Geochemically, the most obvious characteristic of the pore fluids at all seep stations is the significant level of freshening of interstitial waters in the bottom part of the cores, with Cl reaching minimum values of ~200 mM, corresponding to salinities about one third those of Eastern Mediterranean seawater. Porewater freshening in the same range has been reported from the Isis mud volcano in the central part of the Nile deep-sea fan (Feseker et al. 2009b). Typical sources for the addition of fresh water in this type of environment are the release of structurally bound water due to mineral dehydration and gas hydrate decomposition (cf. Dählmann and de Lange 2003; Hensen et al. 2004). Since gas hydrates are not stable at the investigated locations, and because freshening is accompanied by an increase in Na/Cl ratios, we infer that clay mineral dehydration (or more specifically, smectite to illite transformation) is the cause of this porewater freshening. Smectite to illite transformation occurs at temperatures between about 60 and 165°C, and is limited by the availability of potassium (Srodon 1999; Spinelli and Underwood 2004; Cuadros 2006), which may exchange and release varying amounts of sodium from the crystal lattice (Martin et al. 1996; Hensen et al. 2007).

Sediment samples from the mud volcanoes consist of typical mud breccia with clasts of various sizes embedded in a clay/silt matrix. The lower magnetic susceptibility of mud volcano sediments indicates a lower content of magnetic iron oxide minerals, which may be explained by a different origin of the material, or secondary diagenetic processes that lead to dissolution of the iron oxides. The higher bulk density of mud volcano sediments suggests a higher content of terrigenous material, and/or a higher degree of compaction. Both the burial of the source sediments and high pressure in the mud during the ascent to the seafloor could explain the dewatering and reduction of porosity. The increased bulk density of the mud volcano sediments is also accompanied by higher values of thermal conductivity.

### Implications for mud volcano sources

Sediment descriptions show that mud expulsed from the North Alex MV is darker and greener than that from Giza MV. Moreover, down-core measurements of physical properties indicate that sediments from the North Alex MV have lower density and lower magnetic susceptibility (Table 1). These observations point to different source shales with different sediment composition and physical properties.

Even though mud volcano samples have to be considered as reworked material, and no stratigraphic continuity

**Table 3** Concentration in saturated hydrocarbon gas homologues in pore fluids collected below the AOM zone at the centers of North Alex MV and Giza MV

| Core | $CH_4$ (mM) | $C_2H_6$ (μM) | $C_3H_8$ (μM) | $i$-$C_4H_{10}$ (μM) | $n$-$C_4H_{10}$ (μM) | $n$-$C_5H_{12}$ (μM) | $CH_4$/($C_2H_6$+$C_3H_8$) | $n$ |
|---|---|---|---|---|---|---|---|---|
| P362/2–34, Giza MV | 2.4±0.3 | 74±11 | 22±4 | 6±1.6 | 8±2 | <1 | 25±2 | 4 |
| P362/2–100, North Alex MV | 1.2±0.4 | 95±24 | 30±9 | 13±6 | 15±7 | 11±6 | 10±1.4 | 4 |

**Table 4** In-situ sediment temperatures measured using the heatflow probe during the P362/2 cruise of R/V *Poseidon* at a heatflow reference station (P362/2–3), at the center of the Giza MV (P362/2–11 and P362/2–20), and at the center of the North Alex MV (P362/2–44, P362/2–54, P362/2–79, P362/2–87; see Fig. 4 for station locations)[a]

| Sensor | Δz (m) | Temperature (°C) | | | | | | |
|---|---|---|---|---|---|---|---|---|
| | | P362/2–3 | P362/2–11 | P362/2–20 | P362/2–44 | P362/2–54 | P362/2–79 | P362/2–87 |
| 1 | 0.00 | 13.902 | 36.529 | 35.491 | 68.013 | 55.339 | 56.887 | 60.331 |
| 2 | 0.27 | 13.889 | 35.397 | 34.925 | NA | 52.248 | 55.277 | 57.989 |
| 3 | 0.54 | 13.878 | 34.296 | 33.249 | NA | 51.422 | 53.502 | 56.708 |
| 4 | 0.81 | 13.864 | 33.004 | 32.516 | 66.608 | 50.370 | 51.683 | 55.437 |
| 5 | 1.08 | 13.857 | 31.943 | 31.469 | NA | 48.867 | 51.220 | 54.456 |
| 6 | 1.35 | 13.834 | 30.826 | 30.517 | 64.910 | 47.229 | 48.803 | 53.350 |
| 7 | 1.62 | 13.834 | 29.342 | 29.790 | 62.327 | 45.737 | 46.911 | 51.675 |
| 8 | 1.89 | 13.819 | 28.229 | 28.665 | 60.923 | 43.525 | 44.880 | 50.185 |
| 9 | 2.16 | 13.819 | 27.482 | 27.748 | 60.063 | 42.447 | 45.021 | 48.640 |
| 10 | 2.43 | 13.812 | 26.322 | 26.506 | 60.241 | 40.019 | 42.291 | 46.783 |
| 11 | 2.70 | – | – | – | – | – | – | – |
| 12 | 2.97 | 13.791 | 25.071 | 24.494 | 53.813 | 36.009 | – | 42.624 |
| 13 | 3.24 | 13.789 | 24.264 | 23.229 | 51.714 | 33.868 | 35.796 | 40.903 |
| 14 | 3.51 | 13.774 | 23.043 | 22.271 | 50.088 | 32.017 | 26.997 | 38.188 |
| 15 | 3.78 | 13.771 | 22.057 | 21.137 | 46.997 | 30.616 | 22.881 | 36.485 |
| 16 | 4.05 | 13.768 | 20.716 | 20.136 | 44.141 | 28.687 | 13.869 | 34.562 |
| 17 | 4.32 | 13.751 | 19.120 | 19.009 | 40.035 | 25.043 | 13.890 | 33.896 |
| 18 | 4.59 | 13.750 | 17.521 | 17.800 | 34.079 | 23.969 | 13.890 | – |
| 19 | 4.86 | 13.741 | 16.122 | 16.615 | 32.283 | 21.625 | 13.889 | – |
| 20 | 5.13 | 13.744 | 14.773 | 15.439 | 29.255 | 18.970 | 13.890 | – |
| 21 | 5.40 | 13.745 | 14.361 | 14.382 | NA | 16.162 | 13.918 | 21.875 |
| 22 | 5.67 | 13.756 | 13.897 | 13.848 | 15.389 | 14.547 | 13.888 | 14.830 |
| Penetration (m) | | 5.7 | 5.7 | 5.7 | 5.7 | 5.7 | 4.1 | 5.7 |
| Gradient (°C $m^{-1}$) | | 0.032 | 4.03 | 3.92 | 12.07 | 7.13 | 25.89 | 9.70 |

[a] The sediment depth of individual measurements can be obtained by subtracting the sensor offset Δz from the penetration depth. The temperature gradients were calculated for the upper part of the profiles

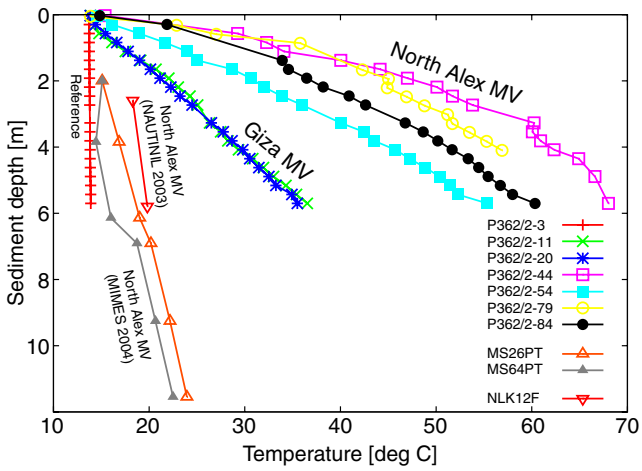


**Fig. 8** In-situ sediment temperature profiles from the central areas of the Giza MV and North Alex MV, and from a reference site a few kilometers from the Giza MV (see Figs. 2 and 4 for station locations)

between successive samples can be assumed or implied, micropaleontological evidence supports the interpretation that the source shales for the Giza MV and North Alex MV appear to be different. The foraminiferal assemblages found in samples from both mud volcanoes are dominated by long-ranging species, and the Pliocene species are the second most abundant group. Compared to samples from the North Alex MV, however, samples from the Giza MV contain a significant number of Miocene species (Fig. 6). The presence of *G. punticulata* in some Giza MV samples is a good indication of the early part of the Late Pliocene (biozone N20, Fig. 5) as an age of deposition, because this species has a short stratigraphic range. Encrusted and deformed specimens from the Middle Miocene (possibly Langhian) in samples from the Giza MV represent reworked material. The nannofossil investigation of the clasts supports this view, with the majority of clasts showing Late Pliocene assemblages. The few clasts that

**Table 5** In-situ thermal conductivity of mud volcano sediments and surrounding seafloor

| Site | Mean thermal conductivity ($W\ K^{-1}\ m^{-1}$) |
|---|---|
| Reference site NW of Giza MV (P362/2–3) | 0.86 |
| Giza MV, moat | 0.87 |
| North Alex MV, flanks | 0.95–0.96 |
| North Alex MV, off-center top | 0.98–1.03 |
| Upslope from North Alex MV | 0.89 |

contain older nannofossils possibly represent fragments of reworked Middle Miocene (NN5?) strata, reworked into later Pliocene sediments. The co-existence of Late Pliocene species (e.g., *G. crassaformis*, *N. acostaensis*) and Early Pleistocene species (e.g., *N. dutertrei*, *N. pachyderma*), along with the absence of *G. punticulata* in samples from the North Alex MV suggest the Late Pliocene (late N21, Fig. 5) as the age of deposition of the source sediments. In contrast to samples from the Giza MV, reworked specimens from the Miocene were not present in samples from the North Alex MV, which supports the interpretation that the sediment sources of the two mud volcanoes are different.

The results of the biostratigraphical analyses of the mud volcano samples were compared to the biostratigraphical log of the Alex-1 well, which is situated about 40 km SSW of the Giza MV at about 200 m water depth. The logs were provided by RWE Dea AG, Germany, and due to proprietary reasons the exact location of the well cannot be given. As shown in Fig. 9, the comparison indicates possible source depths of between 2,100 and 2,450 mbsf for the sediments at the Giza MV (N20), and between 1,150 and 1,550 mbsf for the sediments at the North Alex MV (N21/N22). The Pleistocene species present in all samples from both mud volcanoes are likely to represent material from younger strata that is mixed into older fluidized shale as it rises through the conduit toward the seabed.

Elevated sediment temperatures at shallow depths are controlled by the ambient temperature at the source of the mud volcano, and the heat loss during the ascent of the fluids and mud. The heat loss depends on the diameter and shape of the conduit connecting the source to the seafloor, and the rate of ascent. Applying the regional background geothermal gradient of about 0.032°C $m^{-1}$ (reference heatflow station, P362/2–3) to 0.039°C $m^{-1}$ (reference gravity corer station, P362/2–33) yields temperature ranges of between 80 and 110°C for the sediment source of the Giza MV (Fig. 10). The maximum temperature found in the shallow sediments was about 36°C, suggesting that heat loss during ascent is currently between 50 and 80%. This is less than at the Håkon Mosby mud volcano, where the difference between the maximum temperatures in near-seabed sediments and at the assumed source depth of about 3,000 m corresponds to a heat loss of 85% (Kaul et al. 2006). At the North Alex MV, on the other hand, the estimated temperature at the sediment source is about 50 to 75°C, which is the same range as the temperatures measured in the shallow sediments. In addition, these temperatures are at the lower limit of clay mineral dehydration (Fig. 10). Consequently, the high temperatures near the seabed at the North Alex MV must originate from a warmer fluid source that is significantly deeper than the sediment source, to allow for some heat to be lost during the ascent of the mud.

The interstitial light volatile hydrocarbon gases are highly enriched in heavier homologues (ethane to pentanes), typical of gases produced by thermal cracking of petroleum (Table 3; e.g., Bernard et al. 1978). The association of deep-sourced thermogenic gases and fluids affected by clay mineral dehydration indicates that both phases have migrated from buried strata where they were generated under similar temperature conditions (Powers 1967). Compared to the Giza MV, $CH_4/(C_2H_6+C_3H_8)$ ratios are lower at the center of the North Alex MV, suggesting either that the gases venting at both sites have distinct sources, or that the gases expelled at the Giza MV have experienced more intense post-generational processes such as admixing of shallow archaeal methane, or biodegradation of the heavier homologues (i.e., the gases vented at the center of the North Alex MV have a more "pristine" thermogenic origin). Mastalerz et al. (2007) showed that the hydrocarbon gases vented at the active center of the Isis mud volcano in the eastern Nile deep-sea fan have a mixed thermogenic and microbial source. They suggested that the gas is seeping from a Plio-Pleistocene reservoir, with the

**Table 6** In-situ sediment temperatures and temperature gradients at gravity corer stations. T1, T2, and T3 are the equilibrium temperatures calculated for sensors at 0.46, 2.7, and 4.64 m from the tip of the gravity corer, respectively

| Station no. | Site | T1 (°C) | T2 (°C) | T3 (°C) | Temperature gradient (°C $m^{-1}$) |
|---|---|---|---|---|---|
| P362/2–33 | Reference | 13.882 | 13.795 | 13.718 | 0.039 |
| P362/2–34 | Giza MV center | 20.783 | 15.500 | 14.180 | 1.58 |
| P362/2–100 | North Alex MV center | >55[a] | 53.63 | 33.94 | 10.15 |

[a] At the center of the North Alex MV, the sediment temperature at the lowermost sensor was beyond the detection range of the MTL

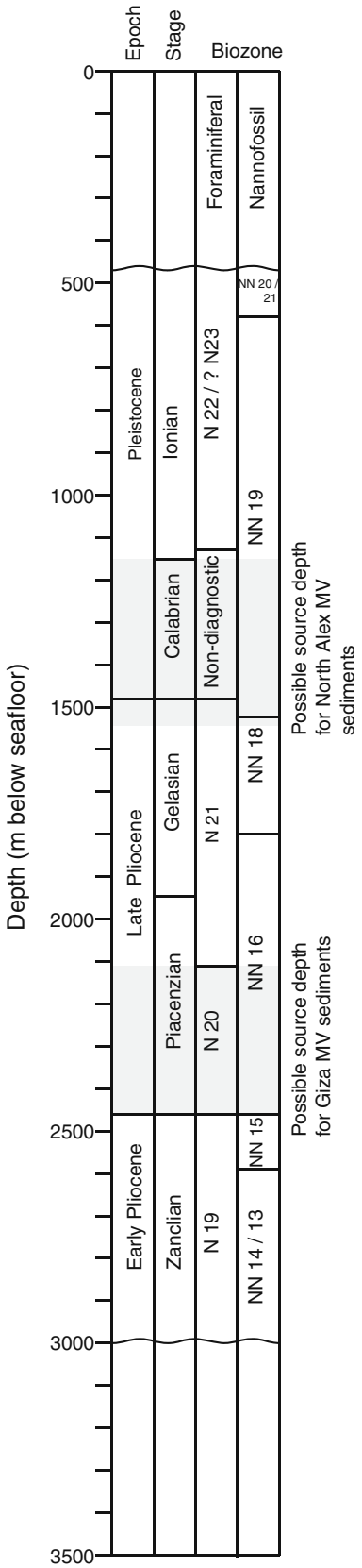


**Fig. 9** Simplified biostratigraphic log of the Alex-1 well, based on data provided by RWE Dea AG. Ranges of possible source depth of sediments from the Giza MV and North Alex MV are marked in *gray*. Foraminiferal N zones follow the scheme of Blow (1969), modified by Bolli and Saunders (1989). Nannofossil NN zonation follows that of Martini (1971), and Berggren et al. (1995)

thermogenic gas having migrated from pre-Pliocene source rocks into the reservoir and microbial methane production taking place within the reservoir. These authors also propose that increasing $CH_4/(C_2H_6+C_3H_8)$ ratios coupled to decreasing $\delta^{13}$C-CH4 values away from the center of the Isis mud volcano occurs as a consequence of diffusive transport of the gas mixture in the buried sediments (Prinzhofer and Pernaton 1997). Mixtures of migrated thermogenic gases and microbial methane produced in situ have likewise been reported from Plio-Pleistocene reservoirs of the western Nile deep-sea fan (Vandré et al. 2007). Our preliminary results are consistent with the conclusions of those previous works in suggesting that the gases vented at the Giza and North Alex mud volcanoes are mainly of thermogenic origin, and have experienced post-generational modification. Compared to the center of the Giza mud volcano, however, the finding of markedly more negative $\delta^{13}$C-CH4 values at the center of the North Alex mud volcano supports the hypothesis that $CH_4$ is furnished by different sources at the two sites.

## Activity of mud volcanoes

As shown in Fig. 7, porewater freshening generally occurs immediately below the $SO_4$ penetration zone, for the North Alex MV at shallower depths than for the Giza MV. Sulfate penetration in these environments is usually driven by anaerobic oxidation of methane (AOM), which is accompanied by a steep increase in alkalinity due to the release of bicarbonate. Thus, the most important control parameters are the methane concentration in the fluids, and the upward flow velocity. Assuming that methane saturation is similar at both sites, shallower $SO_4$ penetration at the North Alex MV compared to the Giza MV therefore indicate higher rates of porewater flow at North Alex, which is in agreement with higher sediment temperatures at these sites. However, the porewater profiles in Fig. 7 reveal more complex dynamics beyond this simple AOM relationship. Above the sulfate-reduction zone, all solute concentration (ratio) profiles (Fig. 7) display bottom water values, indicating bottom water downward mixing possibly caused by hydrocarbon gas ebullition (Haeckel et al. 2007), or density/temperature-driven convection (Henry et al. 1996; Schmidt et al. 2005). Below the sulfate-reduction zone, solute concentrations rapidly change due to different deep fluid chemistry and AOM. Gas bubbling into bottom seawater has been reported at least for the North Alex

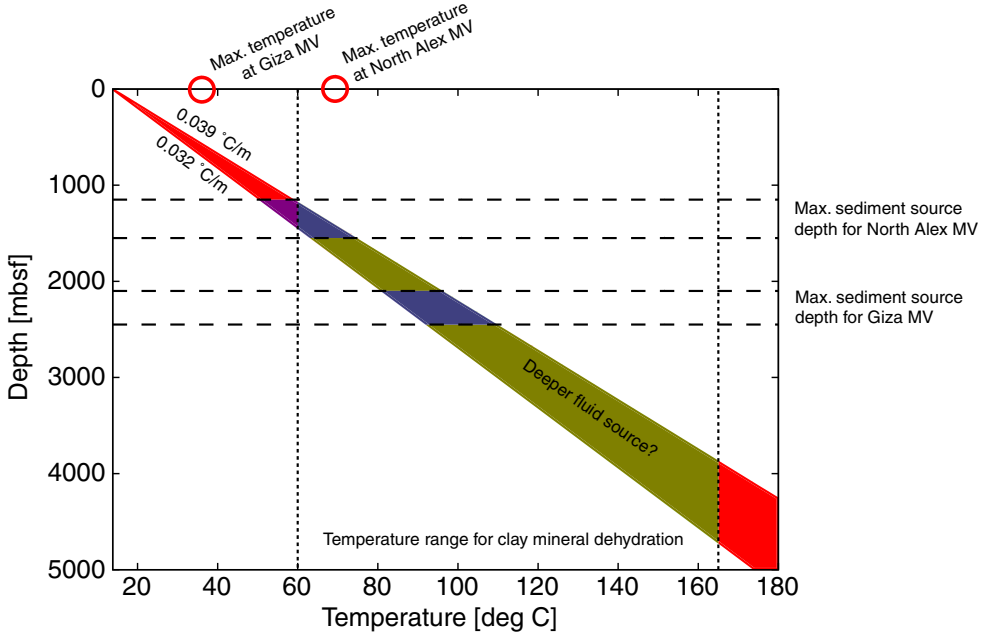


**Fig. 10** Overview of temperatures recorded in shallow sediments of the mud volcanoes and at the estimated source depths, as well as the temperature range required for clay mineral dehydration. The regional background temperature gradient of 0.033–0.039°C $m^{-1}$ points to temperature ranges of 80–110 and 50–75°C at the sediment sources of the Giza MV and North Alex MV, respectively. The temperature difference between shallow sediments of the Giza MV and the estimated source depth suggests a heat loss of 50–80% during mud ascent. The temperatures at the sediment source of the North Alex MV are (1) in the same range and below the temperatures found in shallow sediments, and (2) at the lower limit for clay mineral dehydration, implying warmer fluids from a deeper source

MV (Dupré et al. 2007). The hypothesis of gas bubble ebullition is further supported by the large offset between the $SO_4$ and $CH_4$ profiles at the center of this mud volcano (P362/2–100; Fig. 7): the presence of high amounts of $CH_4$ across the $SO_4$-depletion zone shows that part of the gas is transported upward past the AOM zone, and into the bottom seawater across the sediment-water interface.

Taking sediment temperature as an indicator of mud volcano activity, the North Alex MV was clearly more active, or had been more recently active, than the Giza MV at the time of the P362/2 cruise of R/V *Poseidon* in February 2008. The temperatures in shallow sediments at the Giza MV are in the same range as at other mud volcanoes on the Nile deep-sea fan, such as the Isis mud volcano (Feseker et al. 2009b). In contrast, the extremely high temperatures of up to 70°C measured at the North Alex MV exceed the values reported for any other mud volcano worldwide, as well as the in-situ temperatures recorded during previous expeditions to the North Alex MV in 2003 and 2004 (Fig. 8, Table 4; also see online electronic supplementary material), which were even lower than at the Giza MV. The more recent observations at the Giza MV and North Alex MV may thus reflect two opposite stages in the same range of mud volcano activity. At least the change from a relatively dormant stage—such as the North Alex MV in 2003 and 2004, or Giza MV in 2008—to a highly active stage—such as the North Alex MV in 2008—seems to occur within a few years. The data presently available are insufficient to predict how long an active stage would last, and how quickly the reversal from an active stage to a dormant stage would occur. Observations at the Isis mud volcano suggest that sediment cooling is accelerated by downward infiltration of cold bottom seawater (Feseker et al. 2009b), but only long-term observations will reveal the temporal variability of mud volcanism.

## Conclusions

Giza and North Alex are two active mud volcanoes on the upper slope of the western Nile deep-sea fan. At both sites, fluid emissions are characterized by low chlorinity, most likely due to clay mineral dehydration at the source of the mud volcanoes. The pore fluids contain hydrocarbons that are highly enriched in heavier homologues, indicative of a main thermogenic origin. Anaerobic oxidation of methane is occurring at both mud volcanoes, but the sulfate penetration depth is much smaller at the North Alex MV, pointing to higher rates of upward fluid flow. Porewater profiles reveal sharp transitions from bottom seawater composition to chloride-depleted mud volcano fluids at 50

and 150 cmbsf at the centers of the North Alex and Giza MVs, respectively, hinting at bottom seawater infiltration, possibly due to gas ebullition or buoyancy effects. A wide sulfate-methane transition zone at the center of the North Alex MV supports the interpretation of gas ebullition affecting the geochemical porewater profiles.

Mud breccias from the centers of both mud volcanoes are characterized by increased bulk density and thermal conductivity, possibly as a result of mud transport in the conduit. Biostratigraphic dating of sediment samples yielded depositional ages of Middle Pliocene for the Giza MV, and Late Pliocene to Early Pleistocene for the North Alex MV. According to information on well stratigraphy provided by RWE Dea, the corresponding depths of the mud sources are estimated to be 2,100–2,450 mbsf for the Giza MV, and 1,150–1,550 mbsf for the North Alex MV. Comparison of temperatures measured at shallow depths at the Giza MV and estimates for the temperature range at the mud source indicates that currently at least 50–80% of the heat is lost during ascent of the mud to the seafloor. At the North Alex MV, in contrast, sediment temperatures at shallow depths are in the same range as estimated ambient temperatures at the depth of the mud source, which points to upward migration of warmer fluid from a deeper source before sediment fluidization and mobilization occurs.

Presently available sediment temperature measurements from the P362/2 cruise and from previous research projects show that the activity of the North Alex has been very variable, with rapid changes from dormant to active stages. Even though the Giza MV was less active at the time of the P362/2 cruise, sediment temperatures at the center were higher than at the North Alex MV in 2003 and 2004. Focused on the subsurface structure of these two mud volcanoes, further investigations have been conducted at these sites in the course of the 64PE298-cruise of the Dutch R/V *Pelagia* in November 2008. Notably, uncabled seafloor observatories have been installed to study the dynamics of the Giza and North Alex mud volcano activity over a period of several years.

**Acknowledgements** We would like to thank Captain Michael Schneider and the crew of R/V *Poseidon* for their excellent work at sea, despite the severe weather conditions. Anke Bleyer, Regina Surberg, and Thorsten Schott helped to obtain, prepare, and analyze samples. Wiebke Nehmiz and Gero Wetzel conducted the in-situ temperature and thermal conductivity measurements. Shore-based support by Silke Schenck and Warner Brückmann is gratefully acknowledged. We are indebted to RWE Dea AG, BP Ltd., and Lt. Cdr. Ahmed Kamal Naguib of the Egyptian Hydrographic Office in Alexandria for their kind assistance. Two anonymous reviewers helped to improve the first version of this manuscript and we would like to thank Monique T. Delafontaine for meticulous copy-editing. This work was funded by RWE Dea within the framework of the West Nile Delta Project at IFM-GEOMAR.

## References

Aloisi G, Bouloubassi I, Heijs SK, Pancost RD, Pierre C, Rouchy J-M, Damsté JSS, Gottschal J, Forney LJ, Rouchy J-M (2002) $CH_4$-consumming microorganisms and the formation of carbonate crusts at cold seeps. Earth Planet Sci Lett 203:195–203

Berggren WA, Kent DV, Swisher CC, Aubry M-P (1995) A revised Cenozoic geochronology and chronostratigraphy. In: Berggren WA, Kent DV, Aubry M-P, Hardenbol J (eds) Geochronology, time scales and stratigraphic correlation. SEPM Spec Publ 54:129–212

Bernard BB, Brooks JM, Sackett WM (1978) Light hydrocarbons in recent Texas continental shelf and slope sediments. J Geophys Res 83:4053–4061

Blow WH (1969) Late middle Eocene to Recent planktonic foraminiferal biostratigraphy. In: Bronnimann P, Renz HH (eds) Proc 1st Int Conf Planktonic Microfossils, vol 1, 1967, Geneva. EJ Brill, Leiden, pp 199–422

Bolli HM, Saunders JB (1989) Oligocene to Holocene low latitude planktonic Foraminifera. In: Bolli HM, Saunders JB, Perch-Nielsen K (eds) Plankton stratigraphy, vol 1. Cambridge University Press, Cambridge, pp 155–262

Bouloubassi I, Aloisi G, Pancost RD, Hopmans E, Pierre C, Damsté JSS (2006) Archeal and bacterial lipids in authigenic carbonate crusts from eastern Mediterranean mud volcanoes. Org Geochem 37:484–500

Bowes HL, Hornibrook ERC (2006) Emission of highly $^{13}$C-depleted methane from an upland blanket mire. Geophys Res Lett 33: L04401. doi:10.1029/2005GL025209

Brown KM (1990) The nature and hydrogeologic significance of mud diapirs and diatremes for accretionary systems. J Geophys Res 95 (B6):8969–8982

Bullard EC (1954) The flow of heat through the floor of the Atlantic Ocean. Proc R Soc London, Ser A 222:408–429

Cuadros J (2006) Modeling of smectite illitization in burial diagenesis environments. Geochim Cosmochim Acta 70:4181–4195

Dählmann A, de Lange GJ (2003) Fluid-sediment interactions at Eastern Mediterranean mud volcanoes: a stable isotope study from ODP Leg 160. Earth Planet Sci Lett 212:377–391

de Beer D, Sauter E, Niemann H, Kaul N, Foucher J-P, Witte U, Schlüter M, Boetius A (2006) In situ fluxes and zonation of microbial activity in surface sediments of the Håkon Mosby Mud Volcano. Limnol Oceanogr 52(3):1315–1331

Dupré S, Woodside J, Foucher J-P, de Lange G, Mascle J, Boetius A, Mastalerz V, Stadnitskaia A, Ondréas H, Huguen C, Harmégnies F, Gontharet S, Loncke L, Deville E, Niemann H, Omoregie E, Olu-Le Roy K, Fiala-Medioni A, Dählmann A, Caprais J-C, Prinzhofer A, Sibuet M, Pierre C, Damsté JSS, NAUTINIL Scientific Party (2007) Seafloor geological studies above active gas chimneys off Egypt (Central Nile Deep Sea Fan). Deep-Sea Res, A, Oceanogr Res Pap 54(7):1146–1172

Feseker T, Foucher JP, Harmegnies F (2008) Fluid flow or mud eruptions? Sediment temperature distributions on Håkon Mosby mud volcano, SW Barents Sea slope. Mar Geol 247(3/4):194–207

Feseker T, Pape T, Wallmann K, Klapp SA, Schmidt-Schierhorn F, Bohrmann G (2009a) The thermal structure of Dvurechenskii mud volcano and its implications for gas hydrate stability and eruption dynamics. Mar Petrol Geol 26:1812–1823

Feseker T, Dählmann A, Foucher J-P, Harmegnies F (2009b) In-situ sediment temperature measurements and geochemical porewater data suggest highly dynamic fluid flow at Isis mud volcano, eastern Mediterranean Sea. Mar Geol 261(1/4):128–137

Gieskes JM, Garno T, Brumsack H (1991) Chemical methods for interstitial water analysis aboard Joides Resolution. Ocean

Drilling Program, Texas A & M University, Technical Note 15, College station, TX
Gontharet S, Pierre C, Blanc-Valleron M-M, Rouchy JM, Fouquet Y, Bayon G, Foucher J-P, Woodside J, Mascle J, The Nautinil Scientific Party (2007) Nature and origin of diagenetic carbonate crusts and concretions from mud volcanoes and pockmarks of the Nile deep-sea fan (eastern Mediterranean). Deep-Sea Res II 54 (11/13):1292–1311. doi:10.1016/j.dsr2.2007.04.007
Haeckel M, Boudreau BP, Wallmann K (2007) Bubble-induced porewater mixing: a 3-D model for deep porewater irrigation. Geochim Cosmochim Acta 71:5135–5154
Hedberg HD (1974) Relation of methane generation to undercompacted shales, shale diapirs, and mud volcanoes. AAPG Bull 58 (4):661–673
Henry P, Le Pichon X, Lallemant S, Lance S, Martin JB, Foucher J-P, Fiala-Médioni A, Rostek F, Guilhaumou N, Pranal V, Castrec M (1996) Fluid flow in and around a mud volcano field seaward of the Barbados accretionary wedge: results from Manon cruise. J Geophys Res 101:20297–20323
Hensen C, Wallmann K, Schmidt M, Ranero CR, Suess E (2004) Fluid expulsion related to mud extrusion off Costa Rica continental margin—a window to the subducting slab. Geology 32:201–204
Hensen C, Nuzzo M, Hornibrook E, Pinheiro LM, Bock B, Magalhães VH, Brückmann W (2007) Sources of mud volcano fluids in the Gulf of Cadiz—indications for hydrothermal imprint. Geochim Cosmochim Acta 71:1232–1248
Iaccarino S (1989) Mediterranean Miocene and Pliocene planktonic Foraminifera. In: Bolli HM, Saunders JB, Perch-Nielsen K (eds) Plankton stratigraphy, vol 1. Cambridge University Press, Cambridge, pp 283–314
Ivanenkov VN, Lyakhin YI (1978) Determination of total alkalinity in seawater (in Russian). In: Bordovsky OK, Ivenenkov VN (eds) Methods of hydrochemical investigations in the ocean. Nauka Publ House, Moscow, pp 110–114
Kaul N, Foucher J-P, Heesemann B (2006) Estimating mud expulsion rates from temperature measurements on Håkon Mosby Mud volcano, SW Barents Sea. Mar Geol 229:1–14
Kopf AJ (2002) Significance of mud volcanism. Rev Geophys 40:1005. doi:10.1029/2000RG000093
Loncke L, Gaullier V, Mascle J, Vendeville B (2002) Shallow structure of the Nile deep-sea fan: interactions between structural heritage and salt tectonics; consequences on sedimentary dispersal. In: CIESM (ed) Turbidite systems and deep-sea fans of the Mediterranean and the Black seas. CIESM Workshop Series 17, Monaco
Loncke L, Mascle J, Parties FS (2004) Mud volcanoes, gas chimneys, pockmarks and mounds in the Nile deep-sea fan (eastern Mediterranean): geophysical evidences. Mar Petrol Geol 21:669–689
Loncke L, Gaullier V, Mascle J, Vendeville B, Camera L (2006) The Nile deep-sea fan: an example of interacting sedimentation, salt tectonics, and inherited subsalt paleotopographic features. Mar Petrol Geol 23(3):297–315
Lorenzen J (2009) Nature and origin of fine laminated sediments from the Western Nile Delta: high-resolution elemental content and lithology. Diploma Thesis, Institute of Geosciences, Christian-Albrechts-Universität zu Kiel and IFM-GEOMAR, Kiel, Germany
Martin JB, Kastner M, Henry P, Le Pichon X, Lallement S (1996) Chemical and isotopic evidence for sources of fluids in a mud volcano field seaward of the Barbados accretionary wedge. J Geophys Res 101:20325–20345
Martini E (1971) Standard Tertiary and Quaternary calcareous nannoplankton zonation. In: Farinacci A (ed) Proc II Planktonic Conf, 1970, vol 2, Ed Tecnosci, Rome, pp 739–785
Mascle J, Zitter T, Bellaiche G, Droz L, Gaullier V, Loncke L, Prismed Scientific Party (2001) The Nile deep sea fan: preliminary results from a swath bathymetry survey. Mar Petrol Geol 18:471–477
Mastalerz V, de Lange GJ, Dählmann A, Feseker T (2007) Active venting at the Isis mud volcano, offshore Egypt: origin and migration of hydrocarbons. Chem Geol 246(1/2):87–106
McAullife C (1971) GC determination of solutes by multiple phase equilibration. Chem Tech 1:46–51
Niemann H, Lösekann T, de Beer D, Elvert M, Nadalig T, Knittel K, Amann R, Sauter EJ, Schlüter M, Klages M, Foucher JP, Boetius A (2006) Novel microbial communities of the Haakon Mosby mud volcano and their role as a methane sink. Nature 443 (7113):854–858
Nuzzo M, Hornibrook ERC, Hensen C, Parkes RJ, Cragg BA, Rinna J, Schneider von Deimling J, Sommer S, Magalhães VH, Reitz A, Bruckmann W, Pinheiro LM (2008) Shallow microbial recycling of deep-sourced carbon in Gulf of Cadiz mud volcanoes. Geomicrobiol J 25:283–295
Perch-Nielsen K (1989) Cenozoic calcareous nannofossils. In: Bolli HM, Saunders JB, Perch-Nielsen K (eds) Plankton stratigraphy, vol 1. Cambridge University Press, Cambridge, pp 329–554
Perez-Garcia C, Feseker T, Mienert J, Berndt C (2009) The Håkon Mosby mud volcano: 330 000 years of focused fluid flow activity at the SW Barents Sea slope. Mar Geol 262:105–115
Powers MC (1967) Fluid-release mechanisms in compacting marine mudrocks and their importance in oil exploration. AAPG Bull 51 (7):1240–1254
Prinzhofer A, Pernaton E (1997) Isotopically light methane in natural gas: bacterial imprint or diffusive fractionation? Chem Geol 142:193–200
Reitz A, Haeckel M, Wallmann K, Hensen C, Heeschen K (2007) Origin of salt-enriched pore fluids in the northern Gulf of Mexico. Earth Planet Sci Lett 259:266–282
Sauter EJ, Muyakshin SI, Charlou J-L, Schluter M, Boetius A, Jerosch K, Damm E, Foucher J-P, Klages M (2006) Methane discharge from a deep-sea submarine mud volcano into the upper water column by gas hydrate-coated methane bubbles. Earth Planet Sci Lett 243(3/4):354–365
Schmale O, Greinert J, Rehder G (2005) Methane emission from high-intensity marine gas seeps in the Black Sea into the atmosphere. Geophys Res Lett 32:L07609. doi:10.1029/2004GL021138
Schmidt M, Hensen C, Mörz T, Müller C, Grevemeyer I, Wallmann K, Mau S, Kaul N (2005) Methane hydrate accumulation in "Mound 11" mud volcano, Costa Rica forearc. Mar Geol 216:83–100
Spinelli GA, Underwood MB (2004) Character of sediments entering the Costa Rica subduction zone: implications for partitioning of water along the plate interface. Island Arc 13:432–451
Srodon J (1999) Nature of mixed-layer clays and mechanisms of their formation and alteration. Annu Rev Earth Planet Sci 27:19–53
Stadnitskaia A, Ivanov MK, Blinova V, Kreulen R, van Weering TCE (2006a) Molecular and isotopic variability of hydrocarbon gases from mud volcanoes in the Gulf of Cadiz, NE Atlantic. Mar Petrol Geol 23:281–296
Stadnitskaia AK, Blinova V, Ivanov MK, Baas M, Hopmans E, van Weering TCE, Damsté JSS (2006b) Lipid biomarkers in sediments of mud volcanoes from the Sorokin Trough, NE Black Sea: probable source strata for the erupted material. Org Geochem 38(1):67–83. doi:10.1016/j.orggeochem.2006.08.012
Stainforth RM, Lamb JL, Luterbacher H, Beard JH, Jeffords RM (1975) Cenozoic foraminiferal zonation and characteristics of index forms. University of Kansas Paleontological Institute, Lawrence, KS, Article 62, pp 1–425
The MEDINAUT Shipboard Scientific Party, Pancost RD, Hopmans EC, Damsté JSS (2001) Archeal lipids in Mediterranean cold

seeps: molecular proxies for anaerobic oxidation. Geochim Cosmochim Acta 65(10):1611–1627

Vandré C, Cramer B, Gerling P, Winsemann J (2007) Natural gas formation in the western Nile delta (Eastern Mediterranean): thermogenic versus microbial. Org Geochem 38:523–539

Wallmann K, Drews M, Aloisi G, Bohrmann G (2006) Methane discharge into the Black Sea and the global ocean via fluid flow through submarine mud volcanoes. Earth Planet Sci Lett 248(1/2):544–559

Werne JP, Haese RR, Zitter T, Aloisi G, Bouloubassi I, Heijs S, Fiala-Medioni A, Pancost RD, Sinninghe Damsté JS, de Lange G (2004) Life at cold seeps: a synthesis of biogeochemical and ecological data from Kazan mud volcano, eastern Mediterranean Sea. Chem Geol 205(3/4):367–390